JOURNAL REHABILITÁCIA
--
LCRH - INVITED EXPERIMENTAL
ISSN 0375 – 0922 www.journal.rehabilitacia.sk

Advances in new materials for bone tissue engineering simplifying postoperative rehabilitation: Recent Scientific Breakthroughs

[1]Daniel FURKA, [1,2]Julio A. DUEÑAS SANTANA, [1*] Samuel FURKA.

[1]Comenius University in Bratislava. Faculty of Science, Department of Physical and Theoretical Chemistry, Bratislava, Slovakia.
[2]Scuola Superiore Meridionale. University of Naples Federico II. Naples, Italy.
[3]Chemical Engineering Department. University of Matanzas, Matanzas. Cuba.

**Corresponding author: samuel.furka@uniba.sk*

SUMMARY/ABSTRACT

Introduction: Bone tissue engineering has emerged as a promising field in regenerative medicine, aiming to develop innovative materials and approaches for bone repair and regeneration, which also leads to simplification and searching for new approaches in postoperative rehabilitation. The integration of novel materials into scaffolds and implants plays a crucial role in improving bone tissue engineering strategies. In recent years, scientific research has made significant progress in identifying and characterizing novel materials with superior properties and functionalities.
Aim: This article explores the most recent scientific findings and research breakthroughs concerning novel materials for bone tissues, focusing on their biocompatibility, mechanical properties, bioactivity, and potential clinical applications.
Conclusion: In recent years, the field of bone tissue engineering has witnessed remarkable advancements in the development of novel materials for bone repair and regeneration, which also simplify the medical rehabilitation of the patient. From bioactive glasses and calcium phosphate-based materials to biodegradable magnesium-based materials and graphene-based composites, researchers have explored a wide range of materials with diverse properties and functionalities. As the field continues to evolve, the integration of cutting-edge technologies, including 3D printing and nanotechnology, is expected to further enhance the efficacy and clinical relevance of these novel materials, ultimately benefiting patients with bone defects and diseases.
The experimental scaffold series maintained comparable macroporosity, with mean pore diameters from 238 ± 44 µm to 262 ± 51 µm and total porosity from 67.9 ± 4.1 % to 72.4 ± 4.8 %, providing reproducible geometry for bone-repair scaffold evaluation. HA incorporation reduced the contact angle from 83.2 ± 4.8° to 68.5 ± 5.1° and increased hydrated compressive modulus from 12.6 ± 1.8 MPa to 18.9 ± 2.2 MPa, supporting improved wet-state handling and early low-load support. PolyP45 strengthened the SBF surface response, with day-14 recovered Ca^{2+} concentration of 1.86 ± 0.06 mmol×L^{-1} and mass gain of 6.4 ± 1.0 %, indicating enhanced surface mineral-deposition capacity. Silk-fibroin coating further improved the scaffold interface by reducing the contact angle to 42.7 ± 5.2°, increasing water uptake to 128.0 ± 16.2 %, and preserving hydrated modulus at 22.2 ± 2.6 MPa. The coated scaffold also showed extract viability of 107.5 ± 8.5 % and ALP activity of 1.95 ± 0.27-fold relative to PCL, supporting a favorable preliminary osteoblast-like response. Observed material features support postoperative material selection because protected mobilization, staged loading and patient handling depend on scaffold wetting, wet-state stability and early low-load defect support. The PCL/HA/polyP45-SF group provided the most balanced profile in this series for further preclinical studies linking scaffold-guided repair, postoperative care, recovery-time assessment and personalized selection of bone-repair materials.

KEYWORDS
rehabilitation, operation, artificial bone tissue

DOI: 10.61983/lcrh.v60i3.12

1 INTRODUCTION

Bone tissue engineering has emerged as a promising field in regenerative medicine, aiming to develop innovative materials and approaches for bone repair and regeneration, with potential relevance to postoperative care and rehabilitation planning. The integration of novel materials into scaffolds and implants plays a crucial role in improving bone tissue engineering strategies. In recent years, scientific research has made significant progress in identifying and characterizing novel materials with superior properties and functionalities. Current bone tissue engineering research had increasingly shifted from single-phase materials toward composite scaffolds because individual polymers,

ceramics or hydrogels usually cannot simultaneously fulfil the architectural, mechanical and biological requirements of bone repair[1]. Scaffold performance depends not only on material composition, but also on pore architecture, surface wettability, degradation behavior and mechanical properties[2]. These requirements explain why polymer-ceramic composites became a widely investigated strategy in scaffold design, especially for low-load and non-load-bearing bone-defect models[1,3,4]. Polycaprolactone is a suitable polymeric scaffold matrix because it is processable at relatively low temperature, has thermoplastic behavior and can provide long-term structural support[5]. However, its isolated use is limited by slow degradation and relatively hydrophobic surface character, which may restrict early cell-material interaction[6,7]. For this reason, PCL-based materials are frequently modified or combined with other components to adjust surface wettability, water interactions and biological interface behavior[6–8]. Hydroxyapatite is a logical calcium phosphate component because its apatite structure is chemically related to the substituted and non-stoichiometric carbonated apatite of bone, and it is widely used as an osteoconductive bioceramic[4,9,10]. Its incorporation into polymeric scaffolds can provide calcium phosphate nucleation sites and support mineralization-related processes[11]. A second complementary inorganic component is sodium phosphate glass type 45, polyP45, a Na_2O-P_2O_5-based glass. The aqueous behavior of phosphate-containing inorganic phases depends on composition and medium and can involve dissolution, ion exchange and calcium-phosphate surface reactions[12]. In a PCL/HA scaffold, hydroxyapatite and polyP45 do not act as redundant inorganic fillers. Hydroxyapatite contributes bone-like calcium phosphate chemistry and osteoconductive character, while polyP45 adds a soluble phosphate-glass phase. Previous studies support combined assessment of scaffold architecture, mechanical behavior and SBF-based surface responses in polymer-bioceramic and bioactive-glass composite systems[13–15].

Surface modification with silk fibroin represents another promising strategy[16,17]. Silk fibroin is a natural protein-based biomaterial with favorable biocompatibility, low immunogenicity and adjustable degradation behavior[16,18]. Silk-fibroin coatings have been described as biomaterial surface modifications that can improve cell adhesion, migration and mineralization-related responses. Therefore, the combination of PCL, hydroxyapatite, sodium phosphate glass type 45, polyP45, and silk fibroin was selected as an experimental material-level scaffold model. Interpretation of its biological response requires consideration of the selected osteogenic cell model[19]. The scaffold model connects a slowly degradable structural polymer, an osteoconductive calcium phosphate phase, a soluble phosphate-glass phase and a biofunctional surface coating in one reproducible experimental system, providing a material sequence for selecting compositions according to defect load, surface-response requirements and postoperative handling demands. Simulated body fluid testing is useful as a preliminary assay of apatite-forming surface bioactivity, but it does not prove in vivo osteointegration, implant performance or clinical bone regeneration. Similarly, MG-63 osteoblast-like cells are useful for reduced cytocompatibility screening, but they cannot replace primary human osteoblasts or human mesenchymal stromal cells, because osteoblast-like cell lines may differ from primary cells in proliferation and differentiation-related markers, including alkaline phosphatase activity[19–21]. For this reason, SBF and MG-63-based results should be described as preliminary surface-bioactivity, cytocompatibility and early osteoblast-like assessments[15,19,20,22]. Short-term material stability is also important for scaffold design and postoperative-care planning. A 28-day phosphate-buffered saline stability test can help distinguish early physicochemical stability from surface bioactivity by monitoring mass change, pH drift and preservation of scaffold morphology. Observed parameters provide material-level information relevant to early scaffold handling, local medium stability and the design of gradual low-load testing, but they do not independently define protected-mobilization limits or recovery-time benefits. In future bone-repair studies, scaffold design, recovery medicine and rehabilitation planning should be evaluated together because postoperative loading cannot be inferred from dry-material properties or transferred directly from rigid metallic fixation. For polymer-ceramic systems, ion release, hydration and surface modification may influence the local medium environment before long-term degradation becomes dominant[3,13]. Based on this background, the present study evaluates a composite scaffold series based on polycaprolactone, hydroxyapatite, sodium phosphate glass type 45, polyP45, and regenerated silk fibroin coating, with emphasis on scaffold architecture, wet-state mechanical performance, SBF surface response, PBS stability and preliminary osteoblast-like assessment. The selected endpoints were included to support preliminary comparison of scaffold design and composition for future evaluation in different defect and loading environments, especially in low-load and non-load-bearing bone-repair models.

2 EXPERIMENTAL

2.1 MATERIALS AND METHODS

Poly(ε-caprolactone) (PCL, M_w = 80000 g/mol), synthetic hydroxyapatite nanoparticles (HA, M_w = 502.31 g/mol, particle size <200 nm), sodium phosphate glass type 45 (polyP45, Na_2O-P_2O_5), silk fibroin from domesticated Bombyx mori silkworm supplied as a liquid formulation suitable for cell culture and three-dimensional scaffold applications (50 mg/mL), dichloromethane (CH_2Cl_2, Mw = 84.9 g/mol, anhydrous, ≥99.8 %, containing 40-150 ppm amylene as stabilizer), phosphate-buffered saline (PBS, sterile, pH 7.4), sodium chloride, sodium bicarbonate, potassium chloride, dipotassium hydrogen phosphate trihydrate, magnesium chloride hexahydrate, calcium chloride,

sodium sulfate, TRIS buffer, fetal bovine serum (FBS) and trypsin-EDTA were obtained from Merck and Sigma-Aldrich, USA. Sterile simulated body fluid (SBF, BZ173) was obtained from Biochemazone Ltd., Canada. Ethanol p.a., 70 % ethanol solution and hydrochloric acid were obtained from CENTRALCHEM, s.r.o. DMEM medium was obtained from Thermo Fisher Scientific Inc., USA. MG-63 human osteoblast-like cells were obtained from Cytion GmbH, Germany. Deionized water was prepared using a laboratory-grade reverse-osmosis/deionization system. All chemicals, reagents and cell-culture materials were used as received unless stated otherwise.

Prepared materials and scaffolds were characterized by FTIR, FTIR-ATR, SEM, TEM, BET and SEM/EDS. FTIR and FTIR-ATR spectra were recorded using a Nicolet 6700 FT-IR spectrometer equipped with an ATR accessory (Thermo Scientific, USA) to identify characteristic PCL ester bands, HA and polyP45 phosphate-related bands, and silk-fibroin amide bands. Scaffold morphology, pore architecture and particle distribution were evaluated by SEM using a JSM-7600F field-emission scanning electron microscope (JEOL, Japan) after Au sputter coating, with imaging performed at 10 kV. TEM analysis was performed using a Tecnai G2 F20 transmission electron microscope (FEI, USA) to assess HA nanoparticle morphology and nanoscale inorganic-particle dispersion before scaffold incorporation. BET specific surface area and porous-surface characteristics were determined by nitrogen adsorption-desorption using an ASAP 2020 Plus analyzer (Micromeritics, USA). SEM/EDS analysis was used to evaluate elemental distribution and semi-quantitative Ca/P ratios using an EDS detector coupled to the SEM. Full characterization results are provided in the Supplementary Material. Data are presented as mean ± SD. Each endpoint was measured using seven independently prepared scaffolds per group. Statistical significance was set at $p < 0.05$. Data were evaluated and visualized in OriginPro 2017®. SEM and TEM images were evaluated using ImageJ v1.53 (Release 11/2022).

2.2 PREPARATION OF PCL AND PCL/HA SCAFFOLDS

PCL scaffolds were prepared as the polymeric reference group. PCL was dissolved in anhydrous dichloromethane to obtain a 12 % w/v polymer solution. Sodium chloride particles were added as a particulate porogen at a scaffold-forming solid-to-porogen mass ratio of 1:6. The mixture was homogenized, cast into cylindrical moulds and dried under controlled solvent-evaporation conditions. The obtained cylindrical scaffolds had a diameter of 6 mm and a height of 4 mm. After solvent evaporation, sodium chloride was removed by immersion in deionized water for 48 h, with water replacement every 6 h. The scaffolds were then dried under vacuum for 48 h. Residual dichloromethane in dried scaffolds was checked by headspace GC-FID and remained below 600 ppm.

PCL/HA scaffolds were prepared to evaluate the effect of a calcium-phosphate ceramic phase in the PCL matrix. The scaffold-forming solid phase contained 80 wt% PCL and 20 wt% HA nanoparticles. PCL was dissolved in anhydrous dichloromethane at 12 % w/v, and HA nanoparticles were gradually dispersed into the polymer solution under continuous homogenization. Sodium chloride particles were added as porogen at a scaffold-forming solid-to-porogen mass ratio of 1:6. The mixture was cast into cylindrical moulds, dried under controlled solvent-evaporation conditions, leached in deionized water for 48 h with water replacement every 6 h, and dried under vacuum for 48 h. The same scaffold dimensions and drying conditions as for the PCL reference group were maintained.

2.3 PREPARATION OF PCL/HA/POLYP45 AND PCL/HA/POLYP45-SF SCAFFOLDS

PCL/HA/polyP45 scaffolds were prepared to combine the calcium-phosphate phase with a sodium phosphate-glass phase. The scaffold-forming solid phase contained 75 wt% PCL, 15 wt% HA and 10 wt% polyP45. PCL was dissolved in anhydrous dichloromethane at 12 % w/v. HA nanoparticles and polyP45 powder were dispersed into the PCL solution according to the target formulation. Sodium chloride particles were added as a particulate porogen at a scaffold-forming solid-to-porogen mass ratio of 1:6. The mixture was homogenized, cast into cylindrical moulds and dried under controlled solvent-evaporation conditions. Sodium chloride was removed by immersion in deionized water for 48 h, with water replacement every 6 h. Scaffolds were subsequently dried under vacuum for 48 h. This group was used to evaluate the combined contribution of HA and polyP45 to scaffold morphology, surface chemistry, hydration behavior and in vitro surface response.

PCL/HA/polyP45-SF scaffolds were prepared as the silk-fibroin-coated composite group. The bulk scaffold composition was identical to the PCL/HA/polyP45 group and contained 75 wt% PCL, 15 wt% HA and 10 wt% polyP45. After preparation, leaching and vacuum drying, dry PCL/HA/polyP45 scaffolds were immersed in silk fibroin solution for 2 h. The coated scaffolds were then treated with 70 % ethanol for 30 min to stabilize the silk-fibroin coating. After treatment, the scaffolds were gently rinsed with sterile PBS and dried under controlled conditions. The uncoated PCL/HA/polyP45 scaffold corresponded to 0 % silk-fibroin coating mass gain, while the PCL/HA/polyP45-SF scaffold showed a coating-associated mass gain of 4.8 ± 0.9 %. This group was used to evaluate the effect of silk fibroin surface modification on scaffold wettability, surface morphology and preliminary osteoblast-like cell response.

2.4 PREPARATION OF SAMPLES FOR PHYSICOCHEMICAL AND BIOLOGICAL TESTING

Before physicochemical testing, scaffold samples were dried to constant mass and stored under clean, dry conditions. For hydration, stability and mechanical testing, scaffolds were immersed in PBS at 37 °C according to the specific test protocol. For *in-vitro* surface-bioactivity assessment, scaffolds were immersed in sterile SBF at 37 °C and recovered at defined time points for pH measurement, calcium-ion analysis, mass-change determination and SEM/EDS evaluation. For biological testing, scaffolds were sterilized and preconditioned before contact with MG-63 osteoblast-like cells or before extract preparation. Scaffold extracts were prepared at 0.2 g/mL. MG-63 cells were cultured in DMEM supplemented with FBS under standard cell-culture conditions, and trypsin-EDTA was used for passaging.

3 RESULTS

3.1 3D PRINTING AND ADDITIVE MANUFACTURING

Recent advancements in 3D printing and additive manufacturing have expanded the fabrication of geometrically complex structures for bone tissue engineering[23]. Bioceramics, biodegradable polymers and composite materials can be deposited layer by layer to create controlled and, in selected applications, patient-specific implants and scaffolds[24]. Some 3D-printing and bioprinting approaches also allow the incorporation of growth factors or cells, although biological activity, vascularization, mechanical reliability and clinical translation remain formulation-dependent challenges[25]. These technologies may support more individualized treatment development, but their effects on clinical efficiency and rehabilitation outcomes require direct evaluation. Continuing skeletal growth remains an important design constraint in pediatric applications. The hyperelastic-bone scaffolds described in literature[26,27], were developed for defect-specific bone regeneration, not as structures that autonomously lengthen as a child grows. Effects on repeated operations, quality of life and long-term rehabilitation therefore require separate clinical evaluation.

Controlled scaffold geometry, consistent macroporosity and defined material composition are important requirements for developing porous bone substitutes toward additive-manufacturing-compatible designs. Solvent casting with particulate leaching was used to prepare compositionally defined porous cylinders with fixed dimensions, constant porogen fraction and comparable processing conditions. This allowed the material contribution of PCL, HA, polyP45 and silk fibroin to be evaluated before further optimization by geometry-controlled additive manufacturing. The scaffold series followed the compositional sequence PCL, PCL/HA, PCL/HA/polyP45 and PCL/HA/polyP45-SF. PCL was used as the polymeric reference matrix, HA introduced the calcium-phosphate phase, polyP45 introduced the sodium phosphate-glass phase, and silk fibroin provided the surface coating. This sequence was used to evaluate whether stepwise material modification changed pore architecture, hydrated mechanical response, SBF chemistry, PBS stability and preliminary osteoblast-like response. The scaffold series contained four groups: PCL, PCL/HA, PCL/HA/polyP45 and PCL/HA/polyP45-SF. Magnesium-based materials and graphene-based materials were not included in the quantitative scaffold series because they require separate experimental designs. Magnesium requires corrosion-specific testing, while graphene requires dose, dispersion, oxidation-state and biological-response control. The scaffold compositions are summarized in (Tab. 1).

Table 1. Scaffold groups and composition of the prepared sample scaffolds.

Group	Composition	Surface modification
PCL	100 wt% PCL	None
PCL/HA	80 wt% PCL + 20 wt% HA	None
PCL/HA/polyP45	75 wt% PCL + 15 wt% HA + 10 wt% polyP45	None
PCL/HA/polyP45-SF	75 wt% PCL + 15 wt% HA + 10 wt% polyP45	Silk fibroin coating

The controlled cylindrical geometry, fixed porogen fraction and standardized polymer-ceramic composition provided a material-evaluation step relevant to later additive-manufacturing development. The same scaffold dimensions, leaching procedure and drying procedure were maintained across all groups to ensure that differences between groups were mainly related to composition and surface modification. The pore-size distribution was evaluated by SEM image analysis using equivalent-circle diameters measured from pore contours. For each scaffold group, 160 pores were analyzed. Mean pore diameter was 262 ± 51 μm for PCL, 249 ± 46 μm for PCL/HA, 244 ± 49 μm for PCL/HA/polyP45, and 238 ± 44 μm for PCL/HA/polyP45-SF. Total porosity was 72.4 ± 4.8 %, 70.8 ± 4.5 %, 69.6 ± 4.2 %, and 67.9 ± 4.1 %, respectively. Open porosity was 65.8 ± 4.2 %, 64.9 ± 4.0 %, 63.7 ± 3.8 %, and 62.8 ± 3.7 %, respectively. The mean pore diameters are presented in (Fig. 1A). The box plots show SEM-derived pore-diameter distributions, median values and raw equivalent-circle pore measurements for each scaffold group. The group comparison showed no major difference in mean pore diameter, $p = 0.42$, total porosity, $p = 0.18$, or open porosity, $p = 0.21$. No statistically significant group differences were detected for the reported macroporosity measures, although the analysis does not demonstrate formal equivalence among the groups. The relationship between scaffold relative

density and hydrated compressive modulus is presented in (Fig. 1B). The PCL/HA, PCL/HA/polyP45 and PCL/HA/polyP45-SF groups showed higher hydrated modulus than PCL while maintaining comparable macroporosity. The observed results support the scaffold series as a composition-controlled material-screening platform for later additive-manufacturing optimization. The macroporosity and hydrated-modulus data provide inputs for future low-load testing, but they do not independently define a postoperative loading window, which requires defect-, fixation- and model-specific validation.

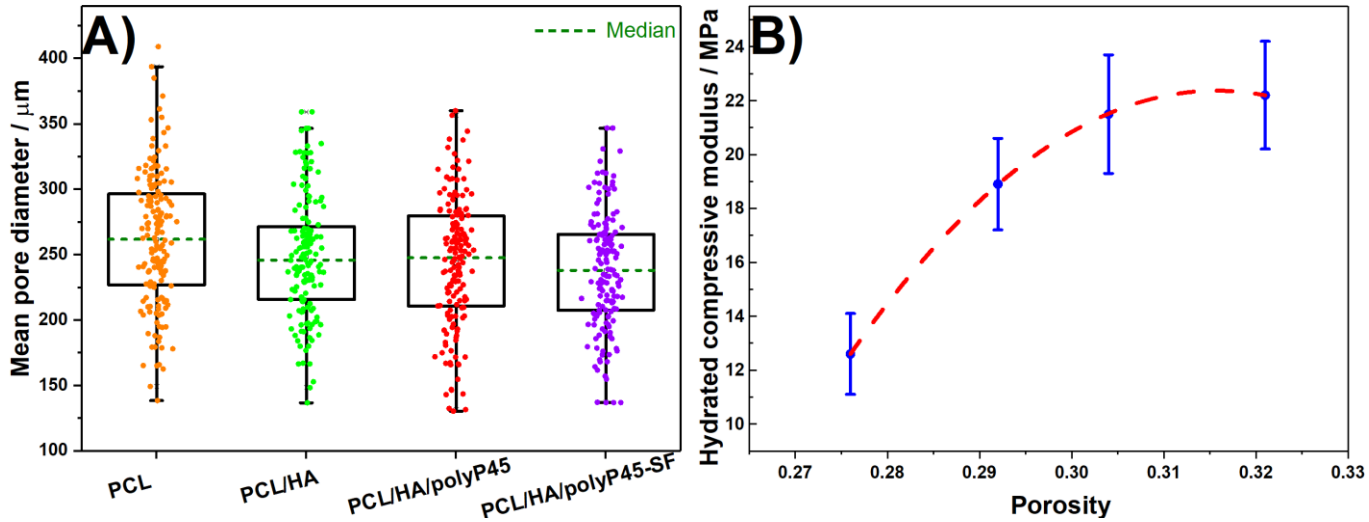


Figure 1. Scaffold architecture and porosity-related mechanical behavior. Panel A shows SEM-derived pore-diameter distributions with box plots, median values and raw equivalent-circle pore measurements. Panel B shows hydrated compressive modulus as a function of scaffold relative density. Macroporous architecture and wet-state mechanical response are material parameters for scaffold handling, low-load support and staged postoperative loading assessment.

3.2 SBF CHEMICAL RESPONSE OF PHOSPHATE-GLASS-CONTAINING SCAFFOLDS

The in vitro response of the scaffold series was evaluated by sterile SBF immersion during a 14-day period. The chemical response was followed using pH of recovered SBF and dissolved Ca^{2+} concentration in recovered SBF. The pH kinetics are presented in (Fig. 2A). SBF pH after 14 days was 7.46 ± 0.03 for PCL, 7.58 ± 0.04 for PCL/HA, 7.72 ± 0.05 for PCL/HA/polyP45, and 7.67 ± 0.05 for PCL/HA/polyP45-SF. The group effect was $p < 0.001$. The calcium-depletion profile is presented in (Fig. 2B). The initial Ca^{2+} concentration in SBF was 2.50 mmol×L^{-1}. After 14 days, recovered Ca^{2+} concentration was 2.41 mmol×L^{-1} for PCL, 2.19 mmol×L^{-1} for PCL/HA, 1.86 mmol×L^{-1} for PCL/HA/polyP45, and 1.81 mmol×L^{-1} for PCL/HA/polyP45-SF. The group effect for day-14 Ca^{2+} concentration was $p < 0.001$. The SBF response was evaluated together with net mass increase and semi-quantitative Ca/P ratio (Tab. 2). Net mass increase after 14 days was 0.8 ± 0.3 % for PCL, 2.9 ± 0.7 % for PCL/HA, 6.4 ± 1.0 % for PCL/HA/polyP45, and 6.9 ± 1.1 % for PCL/HA/polyP45-SF. Semi-quantitative SEM/EDS showed Ca/P ratios of 1.52 ± 0.10 in PCL/HA, 1.58 ± 0.08 in PCL/HA/polyP45, and 1.61 ± 0.07 in PCL/HA/polyP45-SF. The PCL group showed only a weak calcium phosphate signal and was not suitable for reliable Ca/P quantification. The SBF response provides an in vitro comparison of surface precipitation-related behavior and may help prioritize scaffold formulations for further testing, but it does not establish in vivo bone bonding, protected-loading limits or recovery-time effects.

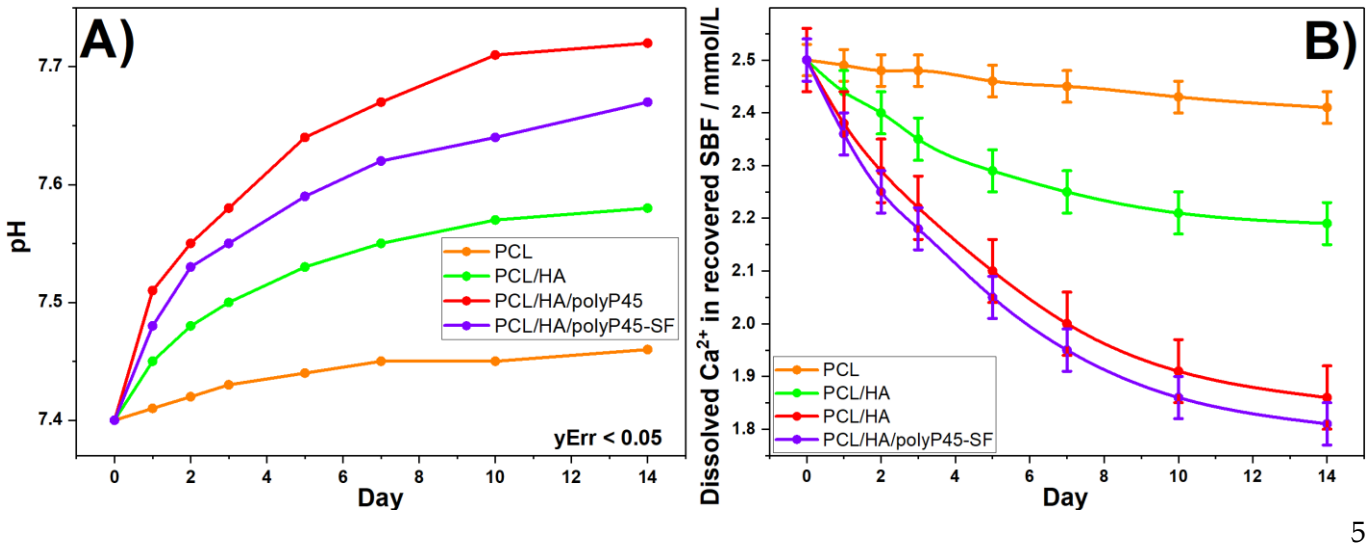


Figure 2. SBF pH kinetics and Ca^{2+} depletion during the in vitro surface-response assessment. Panel A shows pH of recovered SBF during 14-day immersion. Panel B shows dissolved Ca^{2+} concentration in recovered SBF, expressed in mmol×L^{-1}. The figure supports comparison of surface precipitation-related responses before further scaffold-bone contact and loading studies.

Table 2. Chemical response of scaffolds after SBF immersion.

Parameter	PCL	PCL/HA	PCL/HA/polyP45	PCL/HA/polyP45-SF
SBF pH day 14	7.46 ± 0.03	7.58 ± 0.04	7.72 ± 0.05	7.67 ± 0.05
Ca^{2+} in recovered SBF day 14 (mmol×L^{-1})	2.41 ± 0.03	2.19 ± 0.04	1.86 ± 0.06	1.81 ± 0.06
Net mass increase day 14 (%)	0.8 ± 0.3	2.9 ± 0.7	6.4 ± 1.0	6.9 ± 1.1
Semi-quantitative Ca/P ratio by SEM/EDS	Weak signal	1.52 ± 0.10	1.58 ± 0.08	1.61 ± 0.07

3.3 HYDROXYAPATITE-DEPENDENT WETTABILITY AND HYDRATED MECHANICS

The influence of hydroxyapatite loading on apparent surface wettability is presented in (Fig. 3A). Apparent water contact angle was recorded at 5 s after droplet deposition. The contact angle decreased from 83.2 ± 4.8° for PCL to 68.5 ± 5.1° for PCL/HA. The group effect was $p < 0.001$. The influence of hydroxyapatite loading on hydrated compressive modulus is presented in (Fig. 3B). The modulus increased from 12.6 ± 1.8 MPa for PCL to 18.9 ± 2.2 MPa for PCL/HA. Compressive stress at 10 % strain increased from 1.05 ± 0.16 MPa to 1.51 ± 0.21 MPa. The group comparison for hydrated modulus and stress at 10 % strain was $p < 0.001$. The hydroxyapatite-containing scaffold also showed higher water uptake and non-cytotoxic extract response (Tab. 3). Water uptake increased from 58.6 ± 8.7 % in PCL to 73.4 ± 10.2 % in PCL/HA. Extract viability after 24 h was 96.2 ± 6.4 % for PCL and 101.5 ± 7.3 % for PCL/HA. HA-related increases in hydrated modulus and water uptake support further material-level evaluation. Hydrated behavior is relevant to scaffold handling and low-load testing, but defect support and loading tolerance require validation in appropriate preclinical models.

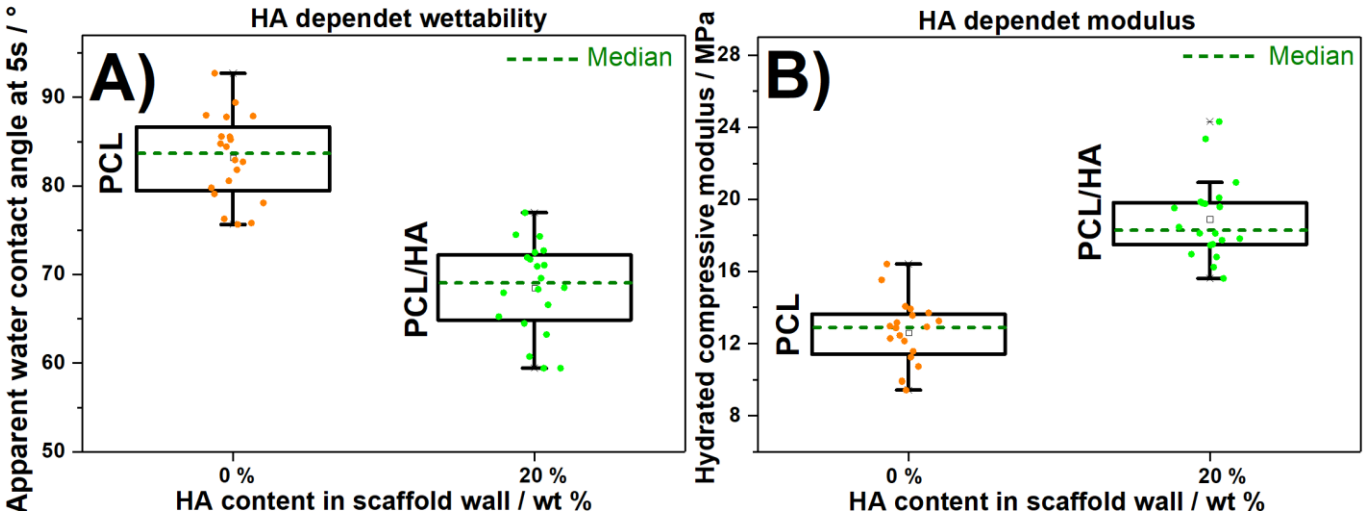


Figure 3. Dependence of wettability and hydrated modulus on hydroxyapatite loading. Panel A shows apparent water contact angle at 5 s as a function of hydroxyapatite content in the scaffold wall. Panel B shows hydrated compressive modulus as a function of hydroxyapatite content. The endpoints support assessment of wet-state handling, low-load support and staged loading tolerance.

Table 3. Hydroxyapatite-related changes in PCL-based scaffolds.

Parameter	PCL	PCL/HA
HA content in scaffold wall (wt%)	0	20
Apparent water contact angle at 5 s (°)	83.2 ± 4.8	68.5 ± 5.1
Water uptake 24 h (%)	58.6 ± 8.7	73.4 ± 10.2
Hydrated compressive modulus (MPa)	12.6 ± 1.8	18.9 ± 2.2
Stress at 10 % strain (MPa)	1.05 ± 0.16	1.51 ± 0.21
Extract viability 24 h (%)	96.2 ± 6.4	101.5 ± 7.3

3.4 PBS STABILITY OF THE POLYMER-CERAMIC SCAFFOLD SERIES

Short-term physicochemical stability of the polymer-ceramic scaffold series was evaluated in PBS during a 28-day period. The PBS pH kinetics are presented in (Fig. 4A), and dry mass-loss kinetics are presented in (Fig. 4B). After 28 days in PBS, pH was 7.39 ± 0.03 for PCL, 7.50 ± 0.05 for PCL/HA, 7.66 ± 0.06 for PCL/HA/polyP45, and 7.60 ± 0.05 for PCL/HA/polyP45-SF. Dry mass loss after 28 days was 1.6 ± 0.4 %, 2.3 ± 0.5 %, 6.3 ± 0.9 %, and 5.4 ± 0.8 %, respectively. The group effect for dry mass loss was $p < 0.001$. The PBS assay provides a short-term

polymer-ceramic stability assessment based on scaffold integrity, pH response and mass retention, supporting material selection for postoperative handling, protected-mobilization studies and staged low-load testing.

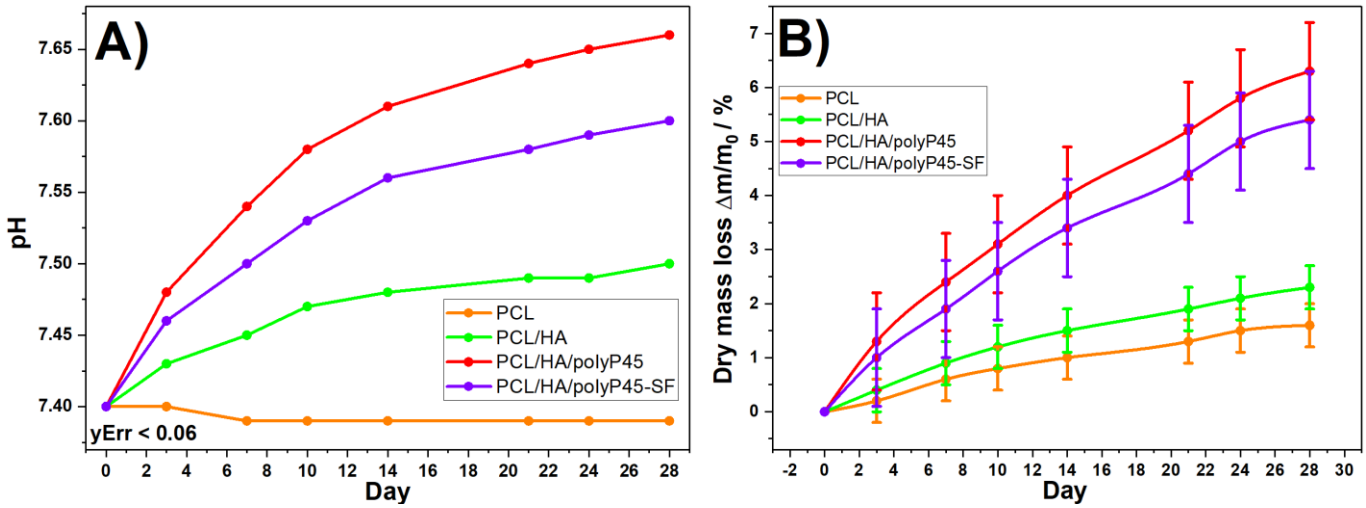


Figure 4. PBS stability of polymer-ceramic scaffolds. Panel A shows pH drift in recovered PBS during 28-day stability screening. Panel B shows dry mass loss expressed as Δm/m0 (%). The data document early pH response and mass retention of polymer-ceramic scaffolds during hydrated stability screening, supporting scaffold selection for subsequent postoperative-handling and staged low-load studies. Error bars represent SD.

Table 4. PBS stability.

Parameter	PCL	PCL/HA	PCL/HA/polyP45	PCL/HA/polyP45-SF
PBS pH day 28	7.39 ± 0.03	7.50 ± 0.05	7.66 ± 0.06	7.60 ± 0.05
Dry mass loss day 28 (%)	1.6 ± 0.4	2.3 ± 0.5	6.3 ± 0.9	5.4 ± 0.8

3.5 SILK-FIBROIN COATING RESPONSE

The PCL/HA/polyP45-SF group was prepared by coating PCL/HA/polyP45 scaffolds with regenerated silk fibroin. The coating-associated mass gain was 4.8 ± 0.9 %. The effect of silk-fibroin coating on apparent wettability is presented in (Fig. 5A), comparing uncoated PCL/HA/polyP45 with silk-fibroin-coated PCL/HA/polyP45-SF. The apparent water contact angle decreased from 58.8 ± 4.7° in PCL/HA/polyP45 to 42.7 ± 5.2° in PCL/HA/polyP45-SF. Water uptake increased from 94.6 ± 12.4 % to 128.0 ± 16.2 %. The group effect was $p < 0.001$. The effect of silk-fibroin coating on relative ALP activity is presented in (Fig. 5B), with values expressed relative to the PCL scaffold group. Relative ALP activity on day 14 increased from 1.76 ± 0.24 in PCL/HA/polyP45 to 1.95 ± 0.27 in PCL/HA/polyP45-SF, with PCL defined as 1.0. Extract viability after 24 h was 103.0 ± 8.0 % for PCL/HA/polyP45 and 107.5 ± 8.5 % for PCL/HA/polyP45-SF. Day-7 metabolic activity increased from 158 ± 16 % to 171 ± 18 %. The silk-fibroin coating preserved hydrated mechanical behavior. Compressive modulus was 21.5 ± 2.5 MPa for PCL/HA/polyP45 and 22.2 ± 2.6 MPa for PCL/HA/polyP45-SF. Modulus retention after cyclic loading was 87.5 ± 4.4 % and 88.9 ± 4.1 %, respectively. The combination of improved wetting, preserved hydrated modulus and a favorable preliminary osteoblast-like response supports selection of the coated scaffold for further low-load bone-repair testing and subsequent protected-mobilization studies requiring stable scaffold handling, maintained wet-state stiffness and a favorable early cell-interface response.

Table 5. Effect of silk fibroin coating on PCL/HA/polyP45 scaffold properties.

Parameter	PCL/HA/polyP45	PCL/HA/polyP45-SF
Silk-fibroin coating mass gain (%)	0 (uncoated)	4.8 ± 0.9 (coated)
Contact angle at 5 s (°)	58.8 ± 4.7	42.7 ± 5.2
Water uptake 24 h (%)	94.6 ± 12.4	128.0 ± 16.2
Compressive modulus (MPa)	21.5 ± 2.5	22.2 ± 2.6
Modulus retention (%)	87.5 ± 4.4	88.9 ± 4.1
Extract viability (%)	103.0 ± 8.0	107.5 ± 8.5
Relative ALP activity at day 14 (PCL = 1.0)	1.76 ± 0.24	1.95 ± 0.27

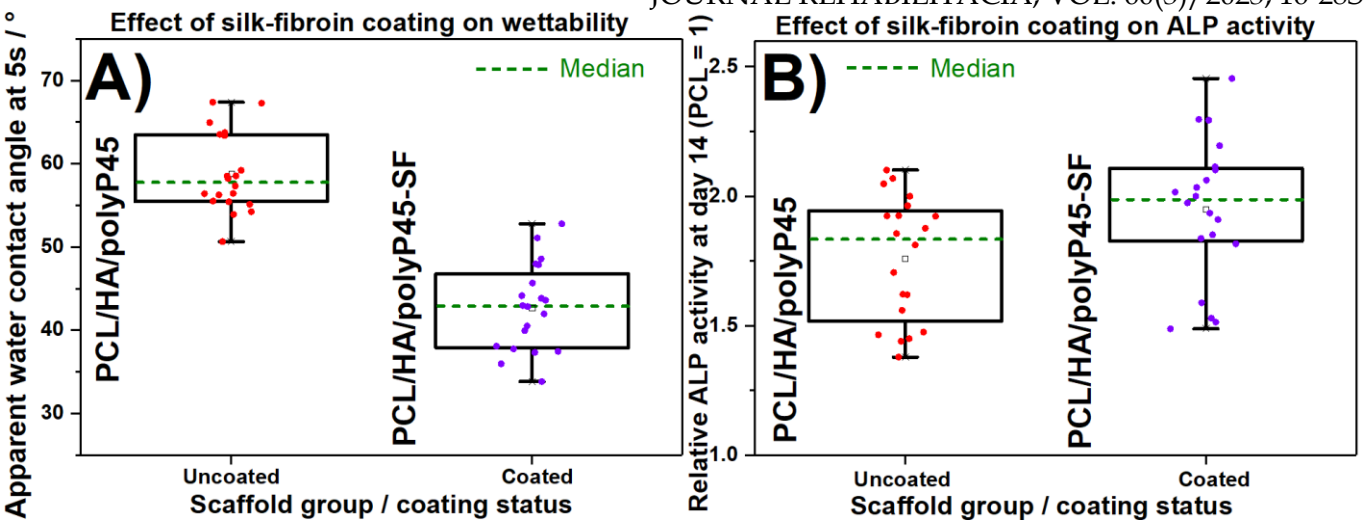


Figure 5. Effect of silk-fibroin coating on scaffold wettability and osteoblast-like response. Panel A compares apparent water contact angle at 5 s for uncoated PCL/HA/polyP45 and silk-fibroin-coated PCL/HA/polyP45-SF scaffolds. Panel B compares relative ALP activity at day 14, expressed relative to the PCL scaffold group. The uncoated scaffold corresponds to 0 % silk-fibroin coating mass gain, while the coated scaffold showed a coating-associated mass gain of 4.8 ± 0.9 %. Surface-interface response and preliminary osteoblast-like activity guide selection of coated scaffolds for protected low-load bone-repair studies.

4 DISCUSSION

4.1 BIOACTIVE GLASSES

Bioactive glasses comprise silicate-, phosphate- and borate-based systems that have garnered significant attention in bone tissue engineering because selected compositions exhibit favorable bioactivity and biocompatibility. Selected bioactive-glass compositions can form a biologically active interfacial layer that supports bonding with surrounding bone tissue, osseointegration and bone regeneration[28]. Recent research has focused on tailoring the composition of bioactive glasses to optimize their mechanical properties, degradation rates, and ion release kinetics. Additionally, bioactive glasses have been investigated beyond bone and dental repair, including applications involving soft-tissue contact and ion-mediated biological responses[29]. The duration and structure of patient rehabilitation should be adapted to defect location, fixation stability, construct mechanics, biological integration and patient-specific factors. Within the broader class of bioactive glasses, silicate-based 45S5 systems are well established, and their biological evaluation depends on glass composition and the selected osteogenic cell model[14,19]. In this scaffold series, polyP45 provided the phosphate-glass component for assessing the dissolution-related SBF response, calcium-consuming surface precipitation and short-term PBS stability in the PCL/HA scaffold system, consistent with previous reports on glass-containing scaffold systems.

The SBF results show that polyP45 changed the chemical response of the PCL/HA scaffold during immersion (Fig. 2). The measurable pH increases in PCL/HA/polyP45 and PCL/HA/polyP45-SF, together with greater Ca^{2+} depletion, higher net mass increase and higher semi-quantitative Ca/P ratios, are consistent with a phosphate-glass-associated surface calcium-phosphate precipitation response (Fig. 2, Tab. 2). The chemical response was evaluated across scaffold groups with similar pore-size and porosity ranges, supporting interpretation of the observed differences primarily in relation to composition and surface modification (Fig. 1, Tab. 1). The PBS data provide complementary stability assessment for the same phosphate-glass-containing scaffolds (Fig. 4). The higher dry mass loss in PCL/HA/polyP45 compared with PCL/HA is consistent with partial dissolution of the sodium phosphate-glass phase, while the slightly lower mass loss and pH drift in PCL/HA/polyP45-SF are consistent with a moderating surface-interface contribution of the silk-fibroin coating (Fig. 4, Tab. 4). Observed findings support the role of polyP45 as a soluble phosphate-glass phase. For postoperative material selection, the SBF response helps identify scaffold surfaces suitable for later scaffold-bone contact testing, protected loading studies and bone-defect repair assessment, where surface mineral deposition can influence the early repair environment (Fig. 2, Tab. 2).

4.2 CALCIUM PHOSPHATE-BASED MATERIALS

Calcium phosphate (CaP) materials, including hydroxyapatite (HA) and tricalcium phosphate (TCP), are well-known for their compositional similarity to the mineral phase of natural bone. Recent research efforts have aimed to tailor the chemistry, handling and mechanical properties of calcium-phosphate materials for bone substitution[30]. For instance, nanocrystalline HA has been developed to enhance the mechanical strength and cellular response of bone scaffolds. Furthermore, researchers have explored the incorporation of silicon and strontium ions into CaP structures, which have shown to enhance osteogenic activity and stimulate bone formation. Because calcium-phosphate

materials provide an osteoconductive environment for bone repair, rehabilitation strategies should account for defect location, fixation stability, scaffold mechanics and expected biological integration. The HA-containing scaffold provides the calcium-phosphate comparison within the PCL-based scaffold series[4,31]. The decrease in apparent static water contact angle and the increase in water uptake indicate improved apparent wettability and hydration after HA incorporation (Fig. 3A, Tab. 3). The increase in hydrated compressive modulus and stress at 10 % strain indicates that HA also improved the compressive response of the scaffold under hydrated conditions (Fig. 3B, Tab. 3). The PCL and PCL/HA groups had comparable macroporous architecture, while PCL/HA showed higher hydrated modulus than PCL (Fig. 1, Fig. 3, Tab. 6). Together, these results support HA as the main mineral contributor to increased hydrated stiffness in the polymer scaffold. For postoperative material selection, higher wet-state stiffness supports scaffold handling during implantation, early low-load defect support and later testing of staged loading conditions, which can influence patient-handling requirements during the protected recovery phase. The MG-63 extract response remained non-cytotoxic and supports further biological assessment (Tab. 3).

4.3 BIODEGRADABLE MAGNESIUM-BASED MATERIALS

Magnesium-based materials have gained interest as biodegradable implant materials for bone repair. Magnesium and selected magnesium alloys combine biodegradability with mechanical properties relevant to temporary structural support[32]. Their biological and mechanical performance is closely linked to alloy composition, corrosion rate and local tissue response. Recent studies have focused on controlling degradation to approximate the required period of mechanical support while limiting rapid corrosion, hydrogen evolution, local alkalization and premature loss of integrity. Alloying and surface modifications have therefore been explored to control corrosion behavior and enhance mechanical performance. Magnesium-based biomaterials belong to a separate biodegradable material class compared with the tested polymer-ceramic scaffold series. Their degradation is controlled mainly by metallic corrosion, surface-passivation behavior, hydrogen evolution, alkalization of the local environment and time-dependent loss of mechanical integrity. The PCL/HA/polyP45/SF scaffold series instead showed changes linked to polymer hydration, calcium-phosphate reinforcement, phosphate-glass dissolution and silk-fibroin surface modification (Fig. 1, Fig. 4). The higher dry mass loss in PCL/HA/polyP45 is consistent with partial dissolution of the sodium phosphate-glass phase, while the lower endpoint mass loss in PCL/HA/polyP45-SF is consistent with a surface-interface contribution of the silk-fibroin coating (Fig. 4B, Tab. 4). PBS pH remained near the physiological range, with a measurable increase in the HA- and polyP45-containing groups. The strongest endpoint shift was observed for PCL/HA/polyP45, while the slightly lower endpoint pH of the silk-fibroin-coated group was consistent with moderation of the phosphate-glass-associated medium response.

4.4 SILK FIBROIN

Silk fibroin, derived from silkworm silk, is a naturally occurring protein with generally favorable biocompatibility and useful mechanical properties. Recent research has demonstrated the potential of silk-fibroin-based scaffolds as carriers for bone growth factors and local drug-delivery systems. Controlled release of bioactive molecules from silk-fibroin scaffolds can support cell adhesion, proliferation and differentiation, thereby contributing to bone-regeneration strategies. Researchers have also combined silk fibroin with calcium phosphates and other polymers to tailor the mechanical and bioactive properties of composite scaffolds[33–35]. Silk fibroin acted as a surface modifier on the PCL/HA/polyP45 scaffold. The coating reduced apparent water contact angle and increased water uptake, showing that silk fibroin changed the surface-interface hydration response (Fig. 5A, Tab. 5). The coated group also showed higher ALP activity and extract viability than the uncoated PCL/HA/polyP45 scaffold, supporting a favorable early osteoblast-like response (Fig. 5B, Tab. 5). Hydrated compressive modulus and modulus retention remained similar between PCL/HA/polyP45 and PCL/HA/polyP45-SF, which indicates that silk fibroin did not act as the main load-bearing reinforcement in this scaffold series (Fig. 5, Tab. 5). For postoperative scaffold design, the profile supports material selection because wetting and preliminary cell-interface response improved while wet-state mechanical stability was preserved during cyclic loading, a combination relevant to subsequent protected-mobilization studies (Fig. 5, Tab. 6).

4.5 GRAPHENE-BASED MATERIALS

Graphene and graphene oxide have attracted substantial interest as modifiers of polymeric, ceramic and composite systems for bone repair. Their high surface area, mechanical properties and electrical behavior provide opportunities to modify scaffold mechanics, surface interactions and cellular responses. A graphene oxide/chitosan/hydroxyapatite composite coating showed favorable wettability, cell adhesion, osteogenic differentiation-related responses and osseointegration on titanium[36]. In recent years, graphene-family materials have been investigated mainly at low concentrations, with their performance governed by material type, oxidation state, loading, lateral dimensions, dispersion quality and scaffold matrix. Reported observations included increased stiffness or compressive response when

graphene-family additives were well dispersed, increased surface roughness or polarity especially for graphene oxide, and improved cell adhesion, proliferation or osteogenic-marker expression in selected in vitro models. These effects depended strongly on graphene type, loading, oxidation state, lateral size, dispersion quality and scaffold matrix. The dose-dependent character of graphene-family materials is important for scaffold design. Low loading was generally associated with more favorable reinforcement and cytocompatibility, while excessive loading or poor dispersion could reduce viability, disturb pore continuity or introduce agglomeration-related heterogeneity. Graphene-based scaffold performance therefore requires material-specific and dose-specific validation. Graphene and graphene oxide were not included in the PCL/HA/polyP45/SF experimental scaffold series, because the present work focused on calcium phosphate incorporation, sodium phosphate-glass response, silk-fibroin surface modification and low-load scaffold stability as primary material requirements for postoperative testing and personalized scaffold selection.

4.6 INTEGRATED PHYSICOCHEMICAL BEHAVIOR OF THE EXPERIMENTAL SCAFFOLD SERIES

The experimental scaffold sequence shows how each added material component changed scaffold architecture, hydration, wet-state mechanics, SBF response, PBS stability and preliminary osteoblast-like response. The comparison starts with PCL as the polymeric reference scaffold, then evaluates the effect of hydroxyapatite addition, sodium phosphate glass incorporation and regenerated silk-fibroin coating. The architecture analysis showed that all four scaffold groups retained comparable macroporous structure, with mean pore diameters between 238 ± 44 μm and 262 ± 51 μm, total porosity between 67.9 ± 4.1 % and 72.4 ± 4.8 %, and open porosity between 62.8 ± 3.7 % and 65.8 ± 4.2 % (Fig. 1, Tab. 6). Separation of composition-related effects from geometry-driven behavior strengthens patient-care translation by linking postoperative loading strategies to wet-state scaffold performance while minimizing confounding effects from uncontrolled pore geometry and assumptions transferred from rigid metallic fixation. The transition from PCL to PCL/HA showed the primary effect of hydroxyapatite incorporation. Apparent water contact angle decreased from 83.2 ± 4.8° to 68.5 ± 5.1°, water uptake increased from 58.6 ± 8.7 % to 73.4 ± 10.2 %, and hydrated compressive modulus increased from 12.6 ± 1.8 MPa to 18.9 ± 2.2 MPa (Fig. 3, Tab. 3). These results show that hydroxyapatite improved apparent wettability, hydration and hydrated stiffness of the polymeric scaffold. In future recovery-time studies, the hydrated-stiffness gain can serve as one material variable for comparing protected-mobilization schedules, patient-handling requirements and staged loading tolerance in low-load bone-defect models. The transition from PCL/HA to PCL/HA/polyP45 showed the additional role of sodium phosphate glass. After 14 days in SBF, pH increased from 7.58 ± 0.04 in PCL/HA to 7.72 ± 0.05 in PCL/HA/polyP45, while recovered Ca^{2+} concentration decreased from 2.19 ± 0.04 mmol×L^{-1} to 1.86 ± 0.06 mmol×L^{-1} (Fig. 2, Tab. 2). Net mass increase rose from 2.9 ± 0.7 % to 6.4 ± 1.0 %, and semi-quantitative Ca/P ratio increased from 1.52 ± 0.10 to 1.58 ± 0.08 (Tab. 2, Tab. 6). Together, these values support a stronger SBF-associated surface calcium-phosphate precipitation response in the phosphate-glass-containing scaffold.

The transition from PCL/HA/polyP45 to PCL/HA/polyP45-SF showed the effect of silk-fibroin surface modification. Apparent water contact angle decreased from 58.8 ± 4.7° to 42.7 ± 5.2°, and water uptake increased from 94.6 ± 12.4 % to 128.0 ± 16.2 % (Fig. 5A, Tab. 5). Hydrated compressive modulus remained similar, with 21.5 ± 2.5 MPa for PCL/HA/polyP45 and 22.2 ± 2.6 MPa for PCL/HA/polyP45-SF. Modulus retention after cyclic loading was also preserved, with 87.5 ± 4.4 % and 88.9 ± 4.1 %, respectively (Fig. 5, Tab. 5). These results support silk fibroin as a surface-interface modifier that improves wetting and hydration while preserving hydrated mechanical performance under the tested conditions. The PBS stability data provides an additional comparison of short-term scaffold behavior outside SBF. After 28 days in PBS, dry mass loss was 1.6 ± 0.4 % for PCL, 2.3 ± 0.5 % for PCL/HA, 6.3 ± 0.9 % for PCL/HA/polyP45, and 5.4 ± 0.8 % for PCL/HA/polyP45-SF (Fig. 4B, Tab. 4). The corresponding PBS pH values were 7.39 ± 0.03, 7.50 ± 0.05, 7.66 ± 0.06, and 7.60 ± 0.05, respectively (Fig. 4A, Tab. 4). The higher mass loss in the sodium-phosphate-glass-containing scaffold is consistent with partial polyP45 dissolution. Early stability supports postoperative-care studies by reducing material-related variability during the first phase of protected low-load assessment, when scaffold handling and local medium stability can influence patient-care requirements. The MG-63 results complemented the physicochemical progression of the scaffold series and strengthened the integrated material comparison. Extract viability remained non-cytotoxic across the scaffold series, with 96.2 ± 6.4 % for PCL, 101.5 ± 7.3 % for PCL/HA, 103.0 ± 8.0 % for PCL/HA/polyP45, and 107.5 ± 8.5 % for PCL/HA/polyP45-SF (Tab. 6). Relative ALP activity at day 14 increased from 1.00 ± 0.16 in PCL to 1.42 ± 0.19 in PCL/HA, 1.76 ± 0.24 in PCL/HA/polyP45, and 1.95 ± 0.27 in PCL/HA/polyP45-SF (Fig. 5B, Tab. 5, Tab. 6). The sequence supports a favorable early osteoblast-like response, while MG-63 cells remain a reduced osteoblast-like model and cannot define complete osteogenic differentiation.

Overall, the experimental observations identify PCL/HA/polyP45-SF as the most balanced material-level scaffold in the tested series. PCL provided the macroporous polymeric matrix, hydroxyapatite reduced apparent water contact angle and increased hydrated modulus, polyP45 increased SBF pH drift, Ca^{2+} depletion and mass gain, and

regenerated silk fibroin further improved apparent wettability and preliminary osteoblast-like response while preserving hydrated mechanical stability (Fig. 1, Fig. 2, Fig. 5, Tab. 6). The observed scaffold response followed a coordinated material sequence: maintained scaffold architecture, improved surface wetting, increased hydrated stiffness, stronger in vitro surface chemical response, controlled PBS stability and non-cytotoxic extract response. For postoperative rehabilitation research, the profile supports material selection for low-load or non-load-bearing bone-defect models in which scaffold handling, protected mobilization, staged loading and recovery-time assessment can be planned in relation to wet-state material behavior. The observed results link bone-scaffold engineering with recovery medicine by identifying material properties relevant to the early repair environment and the design of protection and postoperative-care strategies. PCL/HA/polyP45-SF therefore provides a rational material platform for continued preclinical testing of scaffold-guided repair and postoperative care.

Table 6. Integrated physicochemical comparison of the experimental scaffold series. Values are presented as mean ± SD.

Parameter	PCL	PCL/HA	PCL/HA/polyP45	PCL/HA/polyP45-SF
Mean pore diameter (μm)	262 ± 51	249 ± 46	244 ± 49	238 ± 44
Total porosity (%)	72.4 ± 4.8	70.8 ± 4.5	69.6 ± 4.2	67.9 ± 4.1
Open porosity (%)	65.8 ± 4.2	64.9 ± 4.0	63.7 ± 3.8	62.8 ± 3.7
Apparent water contact angle at 5 s (°)	83.2 ± 4.8	68.5 ± 5.1	58.8 ± 4.7	42.7 ± 5.2
Water uptake 24 h (%)	58.6 ± 8.7	73.4 ± 10.2	94.6 ± 12.4	128.0 ± 16.2
Hydrated compressive modulus (MPa)	12.6 ± 1.8	18.9 ± 2.2	21.5 ± 2.5	22.2 ± 2.6
Stress at 10 % strain (MPa)	1.05 ± 0.16	1.51 ± 0.21	1.72 ± 0.22	1.78 ± 0.23
SBF pH day 14	7.46 ± 0.03	7.58 ± 0.04	7.72 ± 0.05	7.67 ± 0.05
Ca^{2+} in recovered SBF day 14 (mmol×L^{-1})	2.41 ± 0.03	2.19 ± 0.04	1.86 ± 0.06	1.81 ± 0.06
PBS pH day 28	7.39 ± 0.03	7.50 ± 0.05	7.66 ± 0.06	7.60 ± 0.05
PBS dry mass loss day 28 (%)	1.6 ± 0.4	2.3 ± 0.5	6.3 ± 0.9	5.4 ± 0.8
Extract viability 24 h (%)	96.2 ± 6.4	101.5 ± 7.3	103.0 ± 8.0	107.5 ± 8.5
Relative ALP activity at day 14 (PCL = 1.0)	1.00 ± 0.16	1.42 ± 0.19	1.76 ± 0.24	1.95 ± 0.27

5 CONCLUSIONS

In recent years, the field of bone tissue engineering has witnessed remarkable advancements in the development of novel materials for bone repair and regeneration that may contribute to simplifying postoperative rehabilitation. From bioactive glasses and calcium phosphate-based materials to biodegradable magnesium-based materials and graphene-based composites, researchers have explored a wide range of materials with diverse properties and functionalities. As the field continues to evolve, the integration of technologies including 3D printing and nanotechnology may further enhance the efficacy and clinical relevance of these materials and contribute to improved treatment of patients with bone defects and diseases.

The experimental scaffold series maintained comparable macroporosity, with mean pore diameters from 238 ± 44 μm to 262 ± 51 μm and total porosity from 67.9 ± 4.1 % to 72.4 ± 4.8 %, providing controlled and comparable geometry for bone-repair scaffold evaluation. HA incorporation reduced the contact angle from 83.2 ± 4.8° to 68.5 ± 5.1° and increased hydrated compressive modulus from 12.6 ± 1.8 MPa to 18.9 ± 2.2 MPa, supporting improved wet-state handling and subsequent evaluation of early low-load support. PolyP45 strengthened the SBF-associated surface response, with a day-14 Ca^{2+} concentration of 1.86 ± 0.06 mmol×L^{-1} and mass gain of 6.4 ± 1.0 %, consistent with enhanced surface calcium-phosphate precipitation. Silk-fibroin coating further improved the scaffold interface by reducing the contact angle to 42.7 ± 5.2°, increasing water uptake to 128.0 ± 16.2 %, and preserving hydrated modulus at 22.2 ± 2.6 MPa. The coated scaffold also showed extract viability of 107.5 ± 8.5 % and ALP activity of 1.95 ± 0.27-fold relative to PCL, supporting a favorable preliminary osteoblast-like response. Observed material features support selection of PCL/HA/polyP45-SF for further preclinical postoperative testing focused on scaffold wetting, wet-state stability, early low-load support and compatibility with gradual loading. The material profile provides a basis for studies of protected mobilization, staged loading, patient-handling requirements and recovery-time assessment in low-load or non-load-bearing bone-defect models, integrating scaffold engineering with rehabilitation planning.

6 ZUSAMMENFASSUNG

Einleitung: Das Knochengewebe-Engineering entwickelt neue Materialien und Ansätze für Knochenreparatur und Regeneration und beeinflusst damit auch postoperative Rehabilitation und Nachsorge.

Ziel: Der Beitrag bewertet neuartige Materialien für Knochengewebe unter besonderer Berücksichtigung von Biokompatibilität, mechanischen Eigenschaften, Bioaktivität und möglicher klinischer Anwendung.

Schlussfolgerung: Die experimentelle Scaffold-Serie zeigte vergleichbare Makroporosität mit mittleren Porendurchmessern von 238 ± 44 μm bis 262 ± 51 μm und Gesamtporositäten von 67.9 ± 4.1 % bis 72.4 ± 4.8 %. Die HA-Zugabe reduzierte den Kontaktwinkel von 83.2 ± 4.8° auf 68.5 ± 5.1° und erhöhte den hydratisierten Kompressionsmodul von 12.6 ± 1.8 MPa auf 18.9

± 2.2 MPa. polyP45 verstärkte die SBF-Oberflächenantwort, wobei die Ca^{2+}-Konzentration nach 14 Tagen 1.86 ± 0.06 mmol L^{-1} betrug und die Massezunahme 6.4 ± 1.0 % erreichte. Die Seidenfibroin-Beschichtung reduzierte den Kontaktwinkel auf 42.7 ± 5.2°, erhöhte die Wasseraufnahme auf 128.0 ± 16.2 % und erhielt das hydratisierte Modul bei 22.2 ± 2.6 MPa. PCL/HA/polyP45-SF zeigte das ausgewogenste Materialprofil für weitere präklinische Studien zu scaffold-geführter Reparatur, postoperativer Versorgung, stufenweiser Belastung und Erholungszeitbewertung.

REFERENCES

1. Xu, Y. *et al.* Unraveling of Advances in 3D-Printed Polymer-Based Bone Scaffolds. *Polymers* vol. 14 Preprint at https://doi.org/10.3390/polym14030566 (2022).
2. Esmail, A. *et al.* Preparation and characterization of porous scaffolds based on poly(3-hydroxybutyrate) and poly(3-hydroxybutyrate-co-3-hydroxyvalerate). . **11**, (2021).
3. Turnbull, G. *et al.* 3D bioactive composite scaffolds for bone tissue engineering. *Bioactive Materials* vol. 3 Preprint at https://doi.org/10.1016/j.bioactmat.2017.10.001 (2018).
4. Huang, B. *et al.* Polymer-ceramic composite scaffolds: The effect of hydroxyapatite and β-tri-calcium phosphate. *Materials* **11**, (2018).
5. Dwivedi, R. *et al.* Polycaprolactone as biomaterial for bone scaffolds: Review of literature. *Journal of Oral Biology and Craniofacial Research* vol. 10 Preprint at https://doi.org/10.1016/j.jobcr.2019.10.003 (2020).
6. Ferrari, M., Cirisano, F. & Carmen Morán, M. Mammalian cell behavior on hydrophobic substrates: Influence of surface properties. *Colloids and Interfaces* vol. 3 Preprint at https://doi.org/10.3390/colloids3020048 (2019).
7. Saghazadeh, S. *et al.* Drug delivery systems and materials for wound healing applications. *Advanced Drug Delivery Reviews* vol. 127 Preprint at https://doi.org/10.1016/j.addr.2018.04.008 (2018).
8. Solhi, L. *et al.* Understanding Nanocellulose-Water Interactions: Turning a Detriment into an Asset. *Chemical Reviews* vol. 123 Preprint at https://doi.org/10.1021/acs.chemrev.2c00611 (2023).
9. Habibah, T. U., Amlani, D. V. & Brizuela, M. Hydroxyapatite Dental Material. *StatPearls* (2023).
10. Pokhrel, S. Hydroxyapatite: Preparation, Properties and Its Biomedical Applications. *Advances in Chemical Engineering and Science* **08**, (2018).
11. Ielo, I., Calabrese, G., De Luca, G. & Conoci, S. Recent Advances in Hydroxyapatite-Based Biocomposites for Bone Tissue Regeneration in Orthopedics. *International Journal of Molecular Sciences* vol. 23 Preprint at https://doi.org/10.3390/ijms23179721 (2022).
12. Eliaz, N. & Metoki, N. Calcium phosphate bioceramics: A review of their history, structure, properties, coating technologies and biomedical applications. *Materials* **10**, (2017).
13. Poh, P. S. P., Hutmacher, D. W., Stevens, M. M. & Woodruff, M. A. Fabrication and in vitro characterization of bioactive glass composite scaffolds for bone regeneration. *Biofabrication* **5**, (2013).
14. Fiume, E., Barberi, J., Verné, E. & Baino, F. Bioactive glasses: From parent 45S5 Composition to Scaffold-Assisted Tissue-Healing Therapies. *Journal of Functional Biomaterials* vol. 9 Preprint at https://doi.org/10.3390/jfb9010024 (2018).
15. Kokubo, T. & Takadama, H. How useful is SBF in predicting in vivo bone bioactivity? *Biomaterials* **27**, (2006).
16. Wu, R. *et al.* Bioactive Silk Fibroin-Based Hybrid Biomaterials for Musculoskeletal Engineering: Recent Progress and Perspectives. *ACS Applied Bio Materials* vol. 4 Preprint at https://doi.org/10.1021/acsabm.1c00654 (2021).
17. Wu, J. *et al.* Functionalization of Silk Fibroin Electrospun Scaffolds via BMSC Affinity Peptide Grafting through Oxidative Self-Polymerization of Dopamine for Bone Regeneration. *ACS Appl. Mater. Interfaces* **11**, (2019).
18. Nguyen, T. P. *et al.* Silk fibroin-based biomaterials for biomedical applications: A review. *Polymers* vol. 11 Preprint at https://doi.org/10.3390/polym11121933 (2019).
19. Wilkesmann, S. *et al.* Primary osteoblasts, osteoblast precursor cells or osteoblast-like cell lines: Which human cell types are (most) suitable for characterizing 45S5-bioactive glass? *J. Biomed. Mater. Res. A* **108**, (2020).
20. Vandrovcova, M. *et al.* Interaction of human osteoblast-like Saos-2 and MG-63 cells with thermally oxidized surfaces of a titanium-niobium alloy. *PLoS One* **9**, (2014).
21. Chatree, K. *et al.* Distinctions in bone matrix nanostructure, composition, and formation between osteoblast-like cells, MG-63, and human mesenchymal stem cells, UE7T-13. *Heliyon* **9**, (2023).
22. Czekanska, E. M., Stoddart, M. J., Ralphs, J. R., Richards, R. G. & Hayes, J. S. A phenotypic comparison of osteoblast cell lines versus human primary osteoblasts for biomaterials testing. *J. Biomed. Mater. Res. A* **102**, (2014).
23. Furka, S., Furka, D. & Diaz-Pineda, J. Využitie 3D tlače v rehabilitácii – trendy. *REHABILITÁCIA* **56**, 301 (2019).
24. Lin, H. *et al.* Mechanism and application of 3D-printed degradable bioceramic scaffolds for bone repair. *Biomaterials Science* vol. 11 Preprint at https://doi.org/10.1039/d3bm01214j (2023).
25. Zhang, Q. *et al.* 3D printing method for bone tissue engineering scaffold. *Med. Nov. Technol. Devices* **17**, (2023).
26. Alluri, R. *et al.* 3D printed hyperelastic "bone" scaffolds and regional gene therapy: A novel approach to bone healing. *J. Biomed. Mater. Res. A* **106**, (2018).
27. Shokouhimehr, M. *et al.* 3D Bioprinted bacteriostatic hyperelastic bone scaffold for damage-specific bone regeneration. *Polymers (Basel).* **13**, (2021).
28. Jones, J. R. & Hench, L. L. Regeneration of trabecular bone using porous ceramics. *Curr. Opin. Solid State Mater. Sci.* **7**, (2003).
29. Miguez-Pacheco, V., Hench, L. L. & Boccaccini, A. R. Bioactive glasses beyond bone and teeth: Emerging applications in contact with soft tissues. *Acta Biomaterialia* vol. 13 Preprint at https://doi.org/10.1016/j.actbio.2014.11.004 (2015).
30. Zhang, J., Liu, W., Schnitzler, V., Tancret, F. & Bouler, J. M. Calcium phosphate cements for bone substitution: Chemistry, handling and mechanical properties. *Acta Biomaterialia* vol. 10 Preprint at https://doi.org/10.1016/j.actbio.2013.11.001 (2014).
31. Korbut, A. *et al.* Three component composite scaffolds based on PCL, hydroxyapatite, and l-lysine obtained in TIPS-SL: Bioactive material for bone tissue engineering. *Int. J. Mol. Sci.* **22**, (2021).
32. Zhu, Y., Liu, W. & Ngai, T. Polymer coatings on magnesium-based implants for orthopedic applications. *Journal of Polymer Science* vol. 60 Preprint at https://doi.org/10.1002/pol.20210578 (2022).
33. Yan, L. P. *et al.* Bilayered silk/silk-nanoCaP scaffolds for osteochondral tissue engineering: In vitro and in vivo assessment of biological performance. *Acta Biomater.* **12**, (2015).
34. Zuluaga-Vélez, A., Quintero-Martinez, A., Orozco, L. M. & Sepúlveda-Arias, J. C. Silk fibroin nanocomposites as tissue engineering scaffolds – A systematic review. *Biomedicine and Pharmacotherapy* vol. 141 Preprint at https://doi.org/10.1016/j.biopha.2021.111924 (2021).
35. Wu, H., Lin, K., Zhao, C. & Wang, X. Silk fibroin scaffolds: A promising candidate for bone regeneration. *Frontiers in Bioengineering and Biotechnology* vol. 10 Preprint at https://doi.org/10.3389/fbioe.2022.1054379 (2022).
36. Suo, L. *et al.* The enhancement of osseointegration using a graphene oxide/chitosan/hydroxyapatite composite coating on titanium fabricated by electrophoretic deposition. *J. Biomed. Mater. Res. B Appl. Biomater.* **107**, (2019).